Volitional learning promotes theta phase coding in the human hippocampus

Daniel Pacheco Estefan[a,b,c], Riccardo Zucca[b,d,e], Xerxes Arsiwalla[b,c], Alessandro Principe[d,e], Hui Zhang[a], Rodrigo Rocamora[d,e,f], Nikolai Axmacher[a,1], and Paul F. M. J. Verschure[b,c,g,1,2]

[a]Department of Neuropsychology, Institute of Cognitive Neuroscience, Faculty of Psychology, Ruhr University Bochum, 44801 Bochum, Germany; [b]Laboratory of Synthetic Perceptive, Emotive and Cognitive Systems, Institute for Bioengineering of Catalonia, Barcelona Institute of Science and Technology, 08028 Barcelona, Spain; [c]Department of Information and Communications Technologies, Universitat Pompeu Fabra, 08018 Barcelona, Spain; [d]Epilepsy Monitoring Unit, Department of Neurology, Hospital del Mar, 08003 Barcelona, Spain; [e]Hospital del Mar Medical Research Institute, 08003 Barcelona, Spain; [f]Faculty of Health and Life Sciences, Universitat Pompeu Fabra, 08003 Barcelona, Spain; and [g]Institució Catalana de Recerca i Estudis Avançats, 08010 Barcelona, Spain

Edited by Edward T. Bullmore, University of Cambridge, Cambridge, United Kingdom, and accepted by Editorial Board Member Michael S. Gazzaniga January 28, 2021 (received for review October 16, 2020)

Electrophysiological studies in rodents show that active navigation enhances hippocampal theta oscillations (4–12 Hz), providing a temporal framework for stimulus-related neural codes. Here we show that active learning promotes a similar phase coding regime in humans, although in a lower frequency range (3–8 Hz). We analyzed intracranial electroencephalography (iEEG) from epilepsy patients who studied images under either volitional or passive learning conditions. Active learning increased memory performance and hippocampal theta oscillations and promoted a more accurate reactivation of stimulus-specific information during memory retrieval. Representational signals were clustered to opposite phases of the theta cycle during encoding and retrieval. Critically, during active but not passive learning, the temporal structure of intracycle reactivations in theta reflected the semantic similarity of stimuli, segregating conceptually similar items into more distant theta phases. Taken together, these results demonstrate a multilayered mechanism by which active learning improves memory via a phylogenetically old phase coding scheme.

active learning | intracranial EEG | theta oscillations | neural phase coding | hippocampus

Volitionally controlled—or "active"—learning has become a crucial topic in education, psychology, and neuroscience (1, 2). Behavioral studies show that memory benefits from voluntary action (3–5), putatively through a distinct modulation of attention, motivation, and cognitive control (2, 6). While these functions depend on widespread frontoparietal networks (7), a critical role of the hippocampus in coordinating volitional learning has been demonstrated in both humans (8) and rodents (9) (for a review see ref. 10). However, the mechanisms by which volition improves learning and memory are not well understood. Rodent recordings suggest that hippocampal theta oscillations (usually occurring between 4 and 12 Hz) might play a critical role, because they increase during voluntary movement (11) and active sensing (12). Consistently, human studies have shown volition-related theta power increases, although in a lower frequency range (typically between 3 and 8 Hz), during navigation in virtual (13, 14) and physical (15, 16) environments. It is believed that theta oscillations facilitate mnemonic processing by providing a temporal framework for the organization of stimulus-related neural codes (17). This is observed in the phenomenon of phase precession, where spatial locations represented by place cells in the rodent hippocampus are sequentially reactivated at distinct phases of theta oscillations (18). A similar phase coding mechanism underlies the representation of possible future scenarios in rats performing a spatial decision-making task, with early and late hippocampal theta phases representing current and prospective scenarios, respectively (19). It has been proposed (17) that these forms of neural phase coding support a range of cognitive processes, including multi-item working memory (20), episodic memory (21, 22), and mental time travel (23). In humans, this proposal has received empirical support from phase-amplitude coupling studies looking at the relationship between the amplitude of high-frequency activity and the phase of activity at a lower frequency, in particular theta (24–26). However, these analyses are agnostic to the specific content that is coupled to the theta phase and thus do not reflect "phase coding" in the narrower sense. Recent studies used multivariate analysis techniques to identify stimulus-specific representational signals at the high temporal resolution provided by human intracranial electroencephalography data (iEEG, see refs. 27, 28 for review). These analyses demonstrated the relevance of theta oscillations for hippocampal reinstatement of item-context associations (29), for the orchestration of content-specific representations of goal locations (30), and for word-object associations (31). However, it is unclear whether this mechanism is recruited when learning is volitionally controlled.

Building on these empirical findings and methodological advances, we aimed to elucidate whether the improved memory performance typically observed in human active learning paradigms can be traced back to a hippocampal theta phase code. In

Significance

While behavioral evidence shows that volitionally controlled learning benefits human memory, little is known about the neural mechanisms underlying this effect. Insights from spatial navigation research in rodents point to the relevance of hippocampal theta oscillations. However, the mechanisms through which theta might support the beneficial effects of active learning in humans are currently unknown. Here, we demonstrate hippocampal theta oscillations increase during volitional learning, promoting a segregation of task-relevant representational signals according to their semantic content. Our results constitute a direct link to the animal literature on hippocampal theta oscillations and its relation to volition and memory processes.

Author contributions: D.P.E. and P.F.M.J.V. designed research; D.P.E., R.Z., X.A. A.P., H.Z., and R.R. performed research; D.P.E., N.A., and P.F.M.J.V. analyzed data; and D.P.E., N.A., and P.F.M.J.V. wrote the paper.

The authors declare no competing interest.

This article is a PNAS Direct Submission. E.T.B. is a guest editor invited by the Editorial Board.

[1]N.A. and P.F.M.J.V. contributed equally to this work.

[2]To whom correspondence may be addressed. Email: paul.verschure@specs-lab.com.

This article contains supporting information online at https://www.pnas.org/lookup/suppl/doi:10.1073/pnas.2021238118/-/DCSupplemental.

Published March 5, 2021.

particular, we hypothesized that during active learning, this theta phase code organizes and structures stimulus-specific memory representations. We analyzed electrophysiological activity from the hippocampus and widespread neocortical regions in epilepsy patients (n = 13, age = 33.5 ± 9.32) implanted with iEEG electrodes (total number of electrodes = 392; Fig. 1*F*) who performed a virtual reality (VR)-based navigation and memory task. Subjects navigated in a square virtual arena (Fig. 1*A*) and were asked to remember images of specific objects presented at distinct spatial locations indicated by red "boxes" located on the ground (Fig. 1*B*). Images were only visible when participants visited the red boxes and were hidden otherwise. Navigation occurred under two conditions: active (A) and passive (P) (Fig. 1*B*). In the active condition, participants could freely control their movements in visiting the stimulus sites while in the passive condition, they were exposed to the navigation path and order of image presentation generated by another participant (yoked design; Fig. 1 *C* and *D*). At the end of the experiment, the recognition memory for both the actively and passively learned items was tested (Fig. 1*E*). We predicted that active learning would enhance memory by promoting hippocampal theta phase coding of stimulus-specific memory representations.

Results

Active Learning Improves Memory Formation. Across all trials, participants showed a recognition performance of over 80% correct [mean area under the curve: 0.822 ± 0.026, chance level 0.5; W(12) = 91, P = 0.0002; Fig. 1*G*], which was also reflected in their declared confidence [high vs. low confidence trials: W(12) = 91, P = 0.0002, Fig. 1*H*]. Target items were recognized better when they were encoded during active as compared to passive learning conditions [proportion of remembered items: active, 0.8 ± 0.15; passive, 0.65 ± 0.24; W(12) = 74, P = 0.048; 10 out of 13 participants performed better in the active than in the passive condition; Fig. 1 *I*, *Left*]. The proportion of high confidence remembered items differed even more strongly [active, 0.66 ± 0.23; passive, 0.51 ± 0.29; W(12) = 79.5, P = 0.017; 11 out of 13 participants performed better in the active vs. passive condition, Fig. 1 *I*, *Right*]. This was consistent with the performance of a group of healthy subjects (n = 23) following the same paradigm, indicating equivalent enhancement of memory by volition in patients and healthy controls (*SI Appendix*, Fig. S1).

Active Learning Increases Hippocampal Theta Oscillations. Visual inspection of random samples of hippocampal iEEG traces revealed the presence of prominent low-frequency oscillations

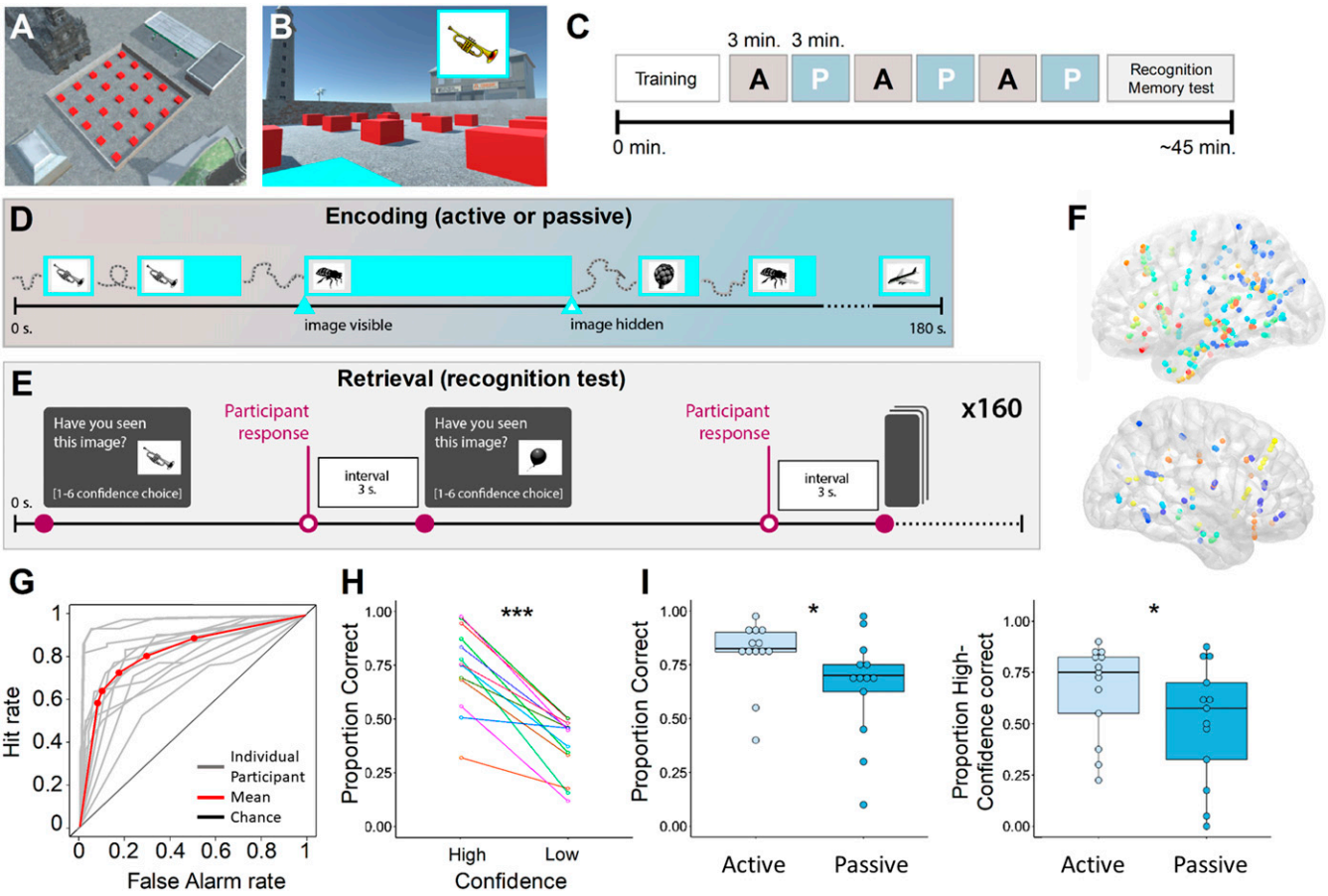

Fig. 1. Experimental procedure, electrode implantation, and behavioral results. (*A*) Participants studied images presented at specific locations, indicated by red boxes located on the ground, in a square virtual environment (here shown from a bird's eye perspective). (*B*) Stimulus presentation during the encoding phase of the experiment as seen by a participant. (*C*) Schematic timeline showing the main blocks of the experiment (A = active, P = passive, counterbalanced). (*D*) Detailed timeline of an example-encoding block. Participants freely determined the timings and materials of study in the active condition and were exposed to the trajectory of a different subject in the passive condition. (*E*) Timeline of the experiment at retrieval. (*F*) All electrodes included in the analyses (n = 392, MNI space), color coded by participant identity. (*G*) Receiver operating characteristic (ROC) curves for each subject (gray) and grand average (red). (*H*) Proportion of correct items for all stimuli as a function of confidence. (*I*) Proportion of remembered items (*Left*) and of high-confidence remembered items (*Right*) for active and passive conditions. *P < 0.05; ***P < 0.001.

during active learning (see Fig. 2*A* for examples from one participant and *SI Appendix*, Fig. S2 for further examples). We quantified the differences in oscillatory power during the encoding phase of our experiment while subjects either controlled their actions in the environment (active condition) or were exposed to the trajectory generated by another participant (passive condition). We observed a significant effect of volition on power in the theta band [$p_{(corrected)} = 0.019$, Fig. 2*B*], while the other bands did not reach significance even at an uncorrected level. Similar results were obtained when we restricted the analysis to the time interval containing item-specific information at encoding [see next section; 250–850 ms; $p_{(corrected)} = 0.018$; Fig. 2*C*]. No significant differences in theta power were observed during retrieval of actively vs. passively encoded items [$W(8) = 13$, $P = 0.3$]. Together, these results show that active learning enhances hippocampal theta oscillations.

Active Learning Increases Item-Specific Memory Reinstatement. Next, we investigated whether active learning affects the precision of item-specific memory reinstatement. To this end, we calculated the similarity between distributed patterns of oscillatory power across all electrodes, frequencies, and time windows. This was done in overlapping time windows of 500 ms, incrementing in steps of 50 ms, for all pairs of encoding and retrieval events ("encoding retrieval similarity" [ERS]; Fig. 3*A*; *Materials and Methods*). In line with previous work (32–34), we found that ERS was significantly higher when the same item was encoded and retrieved as compared to when one item was encoded and a different item retrieved, indicating reinstatement of stimulus-specific representations [$p_{(corrected)} = 0.032$, Fig. 3 *B* and *C*]. This effect could not be explained by semantic similarities among items (*SI Appendix*, Fig. S3). Item-specific ERS started at ∼200 ms after stimulus onset and lasted until ∼800 ms during encoding and retrieval. Importantly, ERS values were higher for items remembered with high confidence as compared to forgotten items within this temporal region of interest [tROI; $W(12) = 75$, $P = 0.039$, Fig. 3*D*], suggesting that they reflect a functionally relevant process. ERS analysis in the subsets of active and passive trials revealed that item-specific information could be extracted in both conditions (*SI Appendix*, Fig. S4). Critically, however, ERS values were higher in active vs. passive trials [$W(12) = 86$, $P = 0.002$, Fig. 3*D* and *SI Appendix*, Fig. S5], and specifically in active trials remembered with high confidence vs. active forgotten trials [$W(8) = 41$, $P = 0.027$, Fig. 3*D* and *SI Appendix*, Fig. S6]. These results indicate that stimulus-specific neural representations are reactivated during successful memory

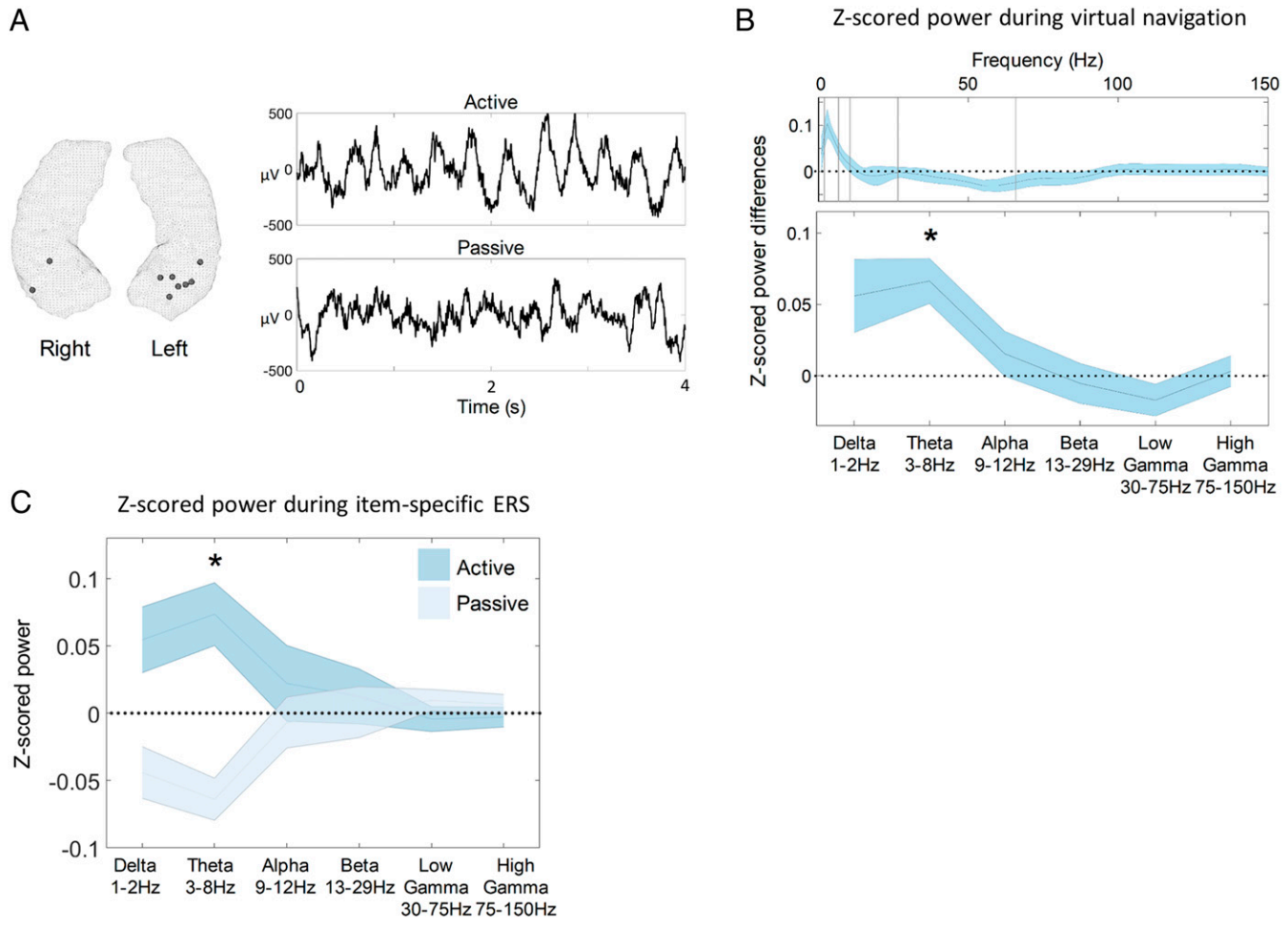

Fig. 2. Active learning increases hippocampal theta oscillations. (*A*) MNI locations of all contacts used in the hippocampal analysis (one per subject, $n = 9$, *Left*). (*Right*) Example hippocampal traces during active (*Top*) and passive (*Bottom*) navigation in one participant, showing a predominance of low-frequency oscillations during active learning (for additional examples, see *SI Appendix*, Fig. S2). (*B*) Z-scored power differences for all frequencies in the 1- to 150-Hz spectrum (*Top*) and across six frequency bands (*Bottom*), showing significantly higher power in the theta band during active vs. passive learning. (*C*) Z-scored power for the active and passive learning conditions during encoding for the interval of significant item-specific encoding retrieval similarity (ERS; 250–850 ms after cue onset). *, $p_{(corrected)} < 0.05$.

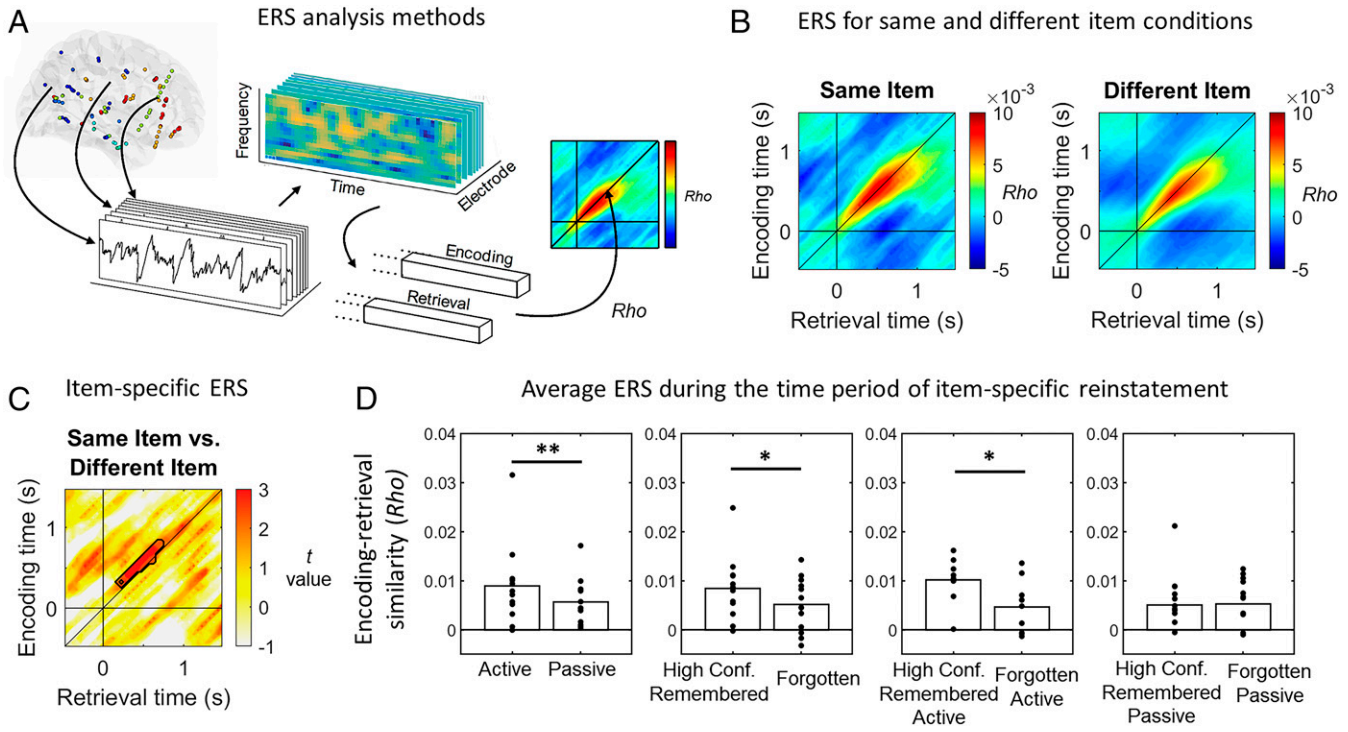

Fig. 3. Active learning increases item-specific reinstatement. (*A*) ERS was calculated using Spearman's correlation (rho) across electrodes, time windows, and frequencies. (*B*) Grand average reinstatement maps for same and different item conditions. (*C*) *T* map of the corresponding contrast in *B* shows item-specific reinstatement from ~200 ms to ~800 ms at both encoding and retrieval (outlined in black; only clusters surviving multiple comparisons corrections are shown). (*D*) Reinstatement of item-specific features is higher for items presented in the active condition and for those remembered with high confidence. Depicted are mean ERS values within the item-specific cluster in *C* for relevant conditions. $*P < 0.05$; $**P < 0.01$.

retrieval, and that the fidelity of this reactivation is increased by volitional learning.

Frequency-Dependent Signatures of Memory Reinstatement. Our results so far indicate that active learning increased hippocampal theta oscillations and enhanced the brain-wide reactivation of stimulus-specific information. We next investigated whether these two phenomena are interrelated. Previous research has linked the role of hippocampal theta oscillations to the coordination of item-specific representations rather than to these representations themselves (8, 29). We therefore evaluated whether theta oscillations contributed to the whole-brain representational patterns we measured during memory retrieval. To this end, we removed activity in the theta band from all electrodes and recalculated item-specific reinstatement. We still found a significant ERS cluster around the same time as in the broadband analysis [$p_{(corrected)} = 0.029$, Fig. 4*A*, *Top* row]. Furthermore, the mean ERS values in the original cluster did not change significantly when excluding the theta frequency band [$W(12) = 55$, $P = 0.54$, Fig. 4*B*]. Finally, when ERS was calculated with information carried only in the theta band, no significant ERS clusters were found (all $P > 0.503$, Fig. 4*A*, *Bottom* row). These results show that item-specific representations do not prominently rely on oscillatory power in the theta frequency range.

To further assess the relevance of specific frequencies to ERS, we correlated the stimulus-induced power changes at each electrode (averaged across trials) during both encoding and retrieval, with the contribution of every electrode to item-specific memory reinstatement (i.e., ERS; *Materials and Methods*). This was done for a broad range of frequencies, because previous studies suggest that fluctuations in various frequencies may reflect the fidelity of stimulus-specific representations (29, 35, 36).

At encoding, we observed a significant correlation between stimulus-induced theta (3–8 Hz) power increases and the contribution of individual electrodes to ERS [$p_{(corrected)} = 0.028$; other frequencies: all $p_{(corrected)} > 0.21$, Fig. 4 *C*, *Left*]. At retrieval, electrode-wise gamma power increases (75–120 Hz) were positively correlated to the contribution of electrodes to ERS [$p_{(corrected)} = 0.014$; cluster-based permutation test, *Materials and Methods*, Fig. 4 *C*, *Right*]. We also observed a negative correlation of beta activity during retrieval and ERS [13–21 Hz; $p_{(corrected)} = 0.019$, Fig. 4 *C*, *Right*].

In summary, these results indicate that electrodes showing pronounced increases of theta power at encoding and gamma power at retrieval, and decreases of beta power at retrieval, contribute most prominently to item-specific reinstatement. Thus, while the brain-wide representations themselves do not rely on theta oscillations, they are dependent on electrodes showing local theta, beta, and gamma effects.

Theta Phase Clustering of Stimulus-Specific Reactivations during Memory Retrieval. A critical question arising from the results presented so far is how hippocampal theta oscillations are mechanistically related to the enhancement of memory performance observed during volitional learning—particularly given that they are not involved in the representation of item-specific information. Since numerous studies in rodents suggest that theta oscillations modulate encoding and retrieval processes (37, 38) and provide a temporal scaffold for phase coding (17, 18), we tested whether similar effects also occur in the human brain. We first investigated whether hippocampal theta phases during encoding and retrieval distinctly modulate ERS. We then asked whether theta oscillations organize the reinstatement of episodic memories according to their representational content.

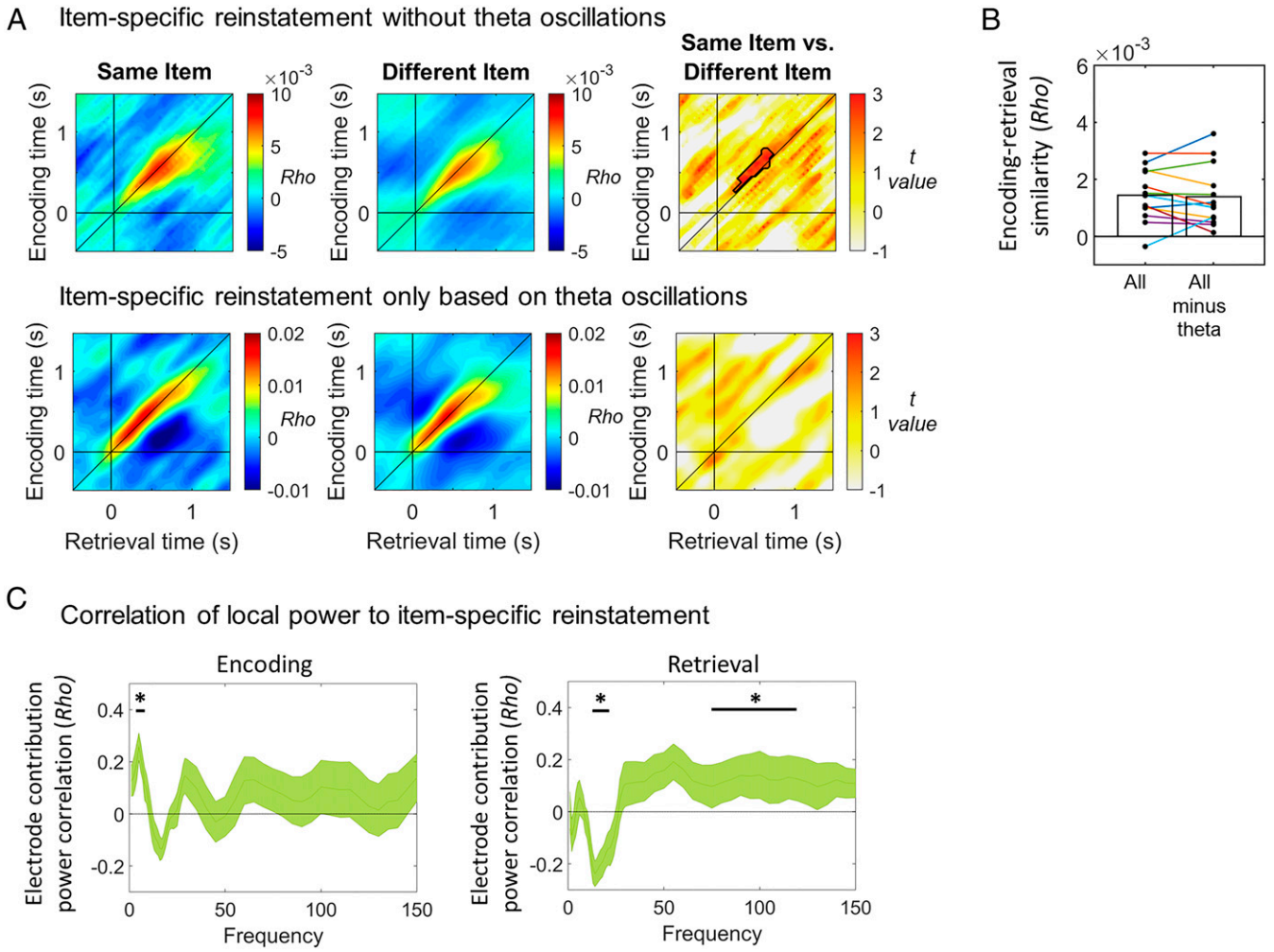

Fig. 4. Frequency profile of item-specific reinstatement. (*A*) Reinstatement analysis after the exclusion of information carried in the theta band revealed a cluster of significant increases in ERS for same as compared to different items, from ~200 to ~750 ms (outlined in black, *Top* row). Analysis performed with information carried only in the theta band did not show any significant cluster of item-specific ERS (*Bottom* row). (*B*) ERS values in the item-specific reinstatement cluster did not drop significantly after excluding theta. (*C*) Correlations between stimulus-related power increases at each electrode and the contribution of these electrodes to stimulus-specific representations were significant in theta (3–8 Hz) at encoding, and in beta (13–21 Hz) and gamma (75–120 Hz) at retrieval. Only clusters surviving multiple comparisons corrections at $P < 0.05$ are shown in *A*. *$P < 0.05$.

For both analyses, we recalculated ERS at an increased temporal resolution (using nonoverlapping windows of 10 ms) and extracted the instantaneous phases of hippocampal 3- to 8-Hz oscillations (Figs. 5*A* and 6*A*, *Left*). In our first analysis, we estimated the theta phase specificity of ERS: We calculated how ERS values changed when information in specific theta phase bins was selectively removed. We considered 20 nonoverlapping phase bins of 18° across the full 360° theta cycle during both encoding and retrieval (Fig. 5*A* and *Materials and Methods*).

During retrieval, removing activity patterns during seven bins between 198° and 324° degrees (corresponding to the rising phase of the oscillation) significantly reduced ERS [$p_{(corrected)} = 0.027$]. Removal of activity at other phase bins did not have an effect (all bins: $P > 0.9$; Fig. 5 *B*, *Top*). These reductions were not dependent on activity at hippocampal channels, as they still occurred when ERS was calculated without hippocampal electrodes [$W(8) = 45$, $P = 0.0039$].

During encoding, no significant relationship between item-specific activity and individual theta phases was found. However, ERS reductions were most pronounced when activity was removed at phases that were opposite to those observed during retrieval [angular mean difference = 160.2°, $F(8) = 6.3$, $P = 0.0084$; Fig. 5*B*].

To test for a possible interaction between theta phase and encoding vs. retrieval, we built a two-way repeated-measures ANOVA with "theta phase" (20 bins) and "memory stage" (encoding vs. retrieval) as factors. This revealed a significant interaction [$F(2, 8) = 1.97$, $P = 0.01$]. To study the influence of volition on the phase of pattern reactivation, we tested whether active and passive phase-ERS distributions differed significantly in their angular means. We found a marked difference at retrieval [angular mean active: 228.3°, angular mean passive: 281°; $F(8) = 11.3$, $P = 0.0007$], while this was not the case at encoding [$F(8) = 0.18$, $P = 0.83$]. For both active and passive trials, phase-ERS distributions at encoding and retrieval showed different angular means [active encoding vs. active retrieval: $F(8) = 10.7$, $P = 0.0008$; passive encoding vs. passive retrieval: $F(8) = 7.9$ $P = 0.003$].

Together, these results demonstrate that item-specific reinstatement during retrieval relies on activity at distinct phases of hippocampal theta oscillations. They further show that these relevant theta phases are significantly shifted when information has been encoded volitionally.

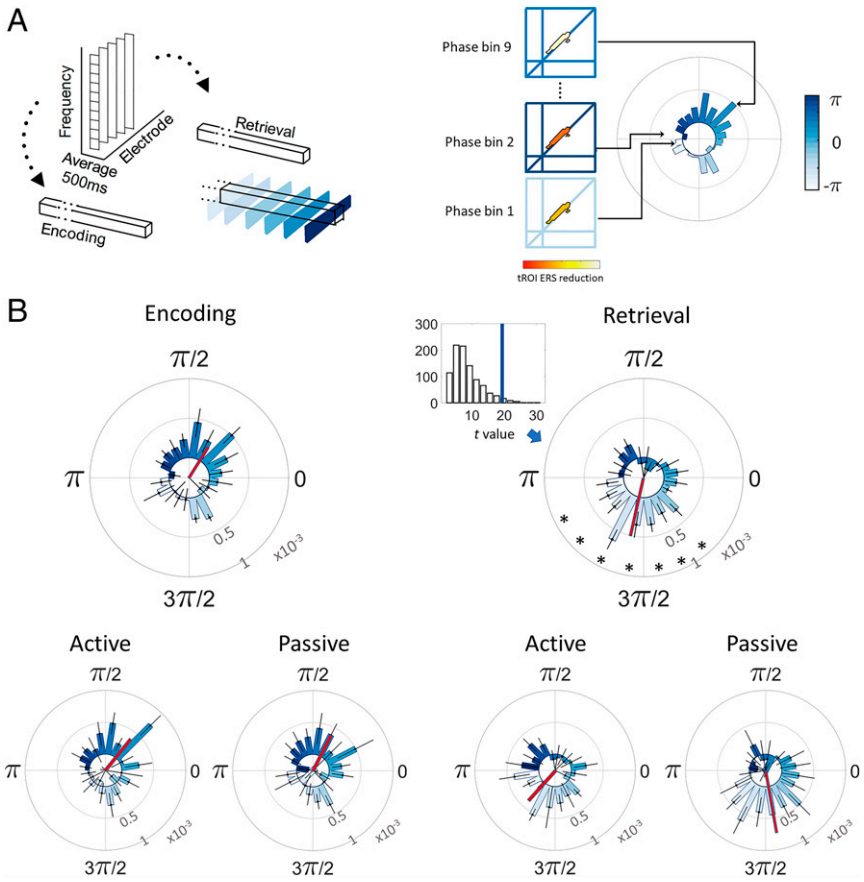

Fig. 5. Theta phase clustering of item-specific memory reinstatement. (*A*) Information at distinct hippocampal theta phases was removed from ERS vectors (separately at encoding and retrieval, *Left*), and ERS reductions were calculated for each phase bin (different shades of blue represent different phase bins; *Right*). (*B*) Clustering of ERS signals carrying item-specific information at encoding (*Left*) and retrieval (*Right*) for all trials (*Top*) and separately for active and passive learning conditions (*Bottom*). Associated *Inset* figure in the retrieval panel shows the corresponding generated null hypothesis distribution and observed *t* value (blue line). Red line in polar plots of *B* indicates the angular means of the corresponding distributions. *, significant phase bins that survive multiple comparisons correction at $P < 0.05$.

Hippocampal Phase Coding of Semantic Information during Active Learning. Finally, we investigated whether hippocampal theta oscillations provide a temporal scaffold for phase coding during memory reinstatement, i.e., whether stimulus-specific memory reactivations are arranged at specific theta phases according to their content. Since the stimuli used in our study consisted of line drawings with only a few perceptual details, we focused on the semantic content of these items. We built distributions of ERS values along theta phase for each trial (Fig. 6*A*) and calculated the circular correlation between all stimulus pairs (Fig. 6 *B*, *Lower* matrices). In addition, we used a word2vec model (39, 40) to quantify the semantic proximity between all pairs of items (Fig. 6 *B*, *Upper* matrices). Comparing these two measures revealed that semantic similarity between pairs of items was expressed in their time of reactivation along hippocampal theta phase: Conceptually similar items were systematically segregated into more distant phases ($P = 0.006$, Fig. 6 *C*, *Left*). This effect was most prominent during the time period when the neural representation of items was reinstated (~200–800 ms), but was robust to various factors including the specific time period of interest (0–1 s after cue onset, $P = 0.006$), the number of phase bins used in the analysis (8 bins: $P = 0.009$, 20 bins: $P = 0.042$) and the specific distance metric employed (Kullback–Leibler distance instead of circular correlation: $P = 0.019$). The effect remained when we removed hippocampal channels from the analysis of ERS ($P = 0.008$) and also when we averaged across revisits before constructing phase-ERS distributions ($P = 0.009$). As expected, given that the ERS representational signal is based on encoding retrieval correlations, the effect was not observed during encoding ($P = 0.65$).

To examine whether this phase coding mechanism is modulated by volition, we performed the same analysis separately for active and passive trials. Phase-ERS distributions were significantly shaped by semantic similarity for actively learned items ($P = 0.035$, Fig. 6 *C*, *Middle*). This was not the case in passive trials ($P = 1$, Fig. 6 *C*, *Right*). Together, these results show that the phase-based distance of the neural signatures of memories negatively correlates with their semantic similarity. They further demonstrate the critical role of volition in promoting this form of phase coding.

Discussion

Building on the observation in rodents that active navigation enhances hippocampal theta oscillations and promotes phase coding of information, we investigated how volition affects mnemonic processes in the human brain. By measuring iEEG from epilepsy patients, we observed that active learning increased hippocampal theta oscillations and item-specific memory reinstatement, promoting a distinct organization of memory representations along the phase of hippocampal theta oscillations that mapped the semantic relations among stimuli and maximally segregated encoding and retrieval epochs. These results demonstrate a volition-mediated phase code relying on hippocampal theta oscillations that

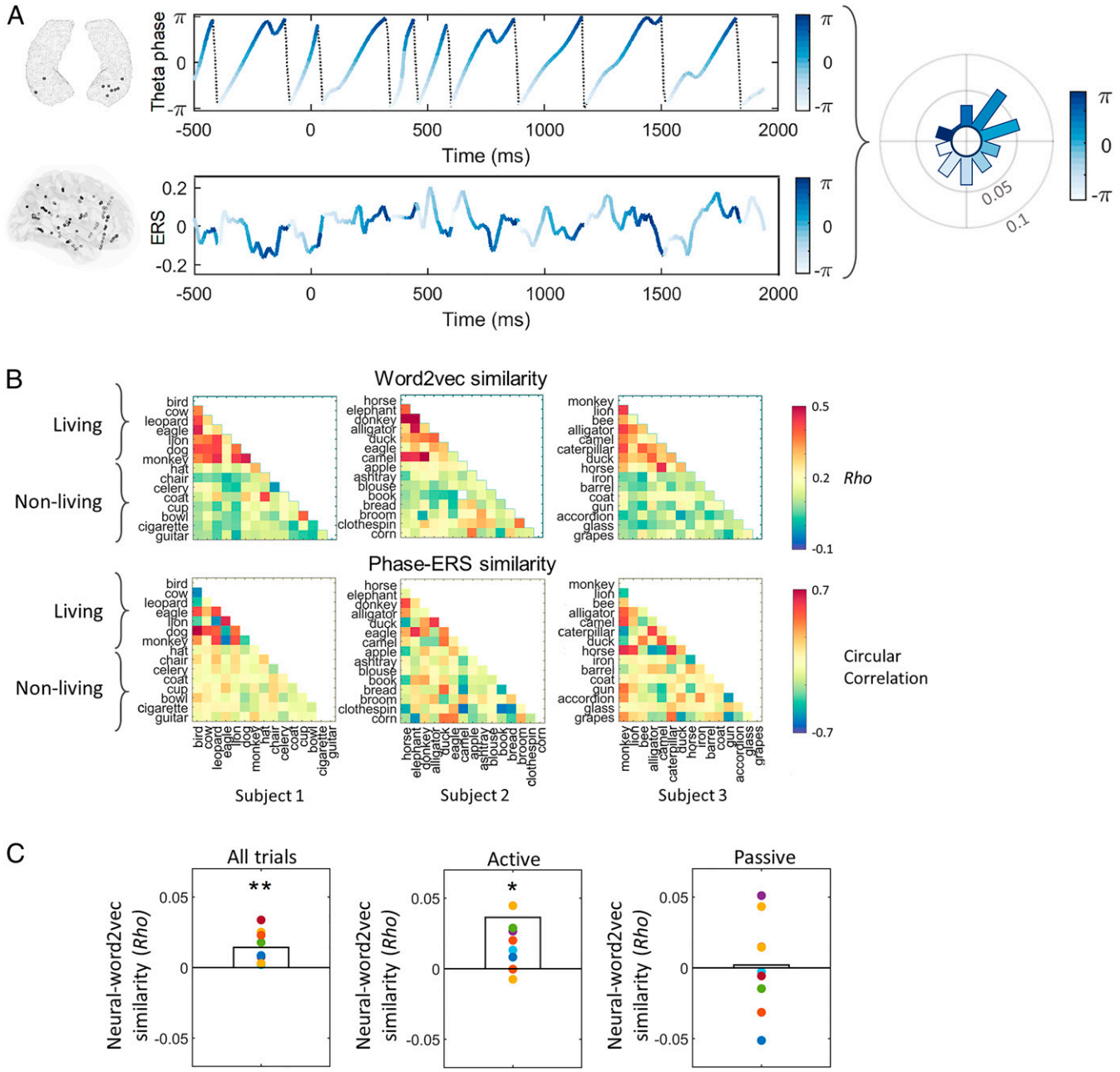

Fig. 6. Active learning promotes hippocampal phase coding of semantic information. (*A*) Analysis strategy. Hippocampal traces were filtered at 3–8 Hz and instantaneous phases were extracted via a Hilbert transform (*Left*, *Top* row). ERS values were sorted depending on the concurrent hippocampal phases (*Left*, *Bottom* row). Single trial phase-ERS distributions were computed (10 equally sized bins covering the full cycle; different shades of blue represent different phase bins; *Right*). (*B*) Pair-wise correlations between word2vec vector representations (*Top*) and phase-ERS distributions (*Bottom*) were calculated for each subject (three examples are shown). Note that by design each participant encoded a different set of images. (*C*) Phase-ERS and word2vec semantic similarities were compared using Spearman's rho. The difference between group-level *t* values and the permutation-based null distribution shows a systematic relationship for active but not for passive trials. Circular correlation values in *B* and rho values in *C* were sign changed for visualization. $*P < 0.05$; $**P < 0.01$.

coordinates and structures brain-wide representational signals during episodic memory.

Our finding that active learning promotes hippocampal theta oscillations constitutes a bridge between long-standing experimental results in the rodent literature and research on human memory. While animal studies reported hippocampal theta power increases during voluntary action (11, 12, 41, 42), this phenomenon has not been established in humans. Previous work demonstrated that hippocampal blood oxygen level-dependent (BOLD) responses track the activity of a brain-wide network underlying volitional learning (8), and that theta power captured at numerous magnetoencephalography (MEG) sensors correlates with self-directed learning and spatial memory (13). Despite these relevant empirical findings, the use of functional magnetic resonance imaging (fMRI) in previous studies (8) does not allow for a precise characterization of hippocampal oscillatory dynamics, and MEG source localization (13) provides only indirect access to the hippocampus. Our data critically complement

these previous results by showing an effect of active learning on hippocampal theta oscillations.

Our results on memory reinstatement are consistent with a growing body of research which has shown that remembering an episode requires the reinstatement of a dynamic oscillatory state in the brain, the "neural fingerprint" of a specific experience (29, 32–34). In addition to replicating the finding of behaviorally relevant item-specific reinstatement (29, 34), our results show that ERS can be actively increased by volitional control over learning (Fig. 3*C*). The use of time-resolved representational signals in our encoding retrieval similarity analyses further allowed us to evaluate phase coding without having to assume that high-frequency activity is a proxy for the representation of specific content, extending previous studies (20, 25, 26).

Our analyses based on hippocampal theta phase revealed a twofold mechanism that simultaneously segregates semantic similarities of item representations and defines optimal oscillatory phases for their encoding and retrieval. Similar phenomena of theta phase coding have been previously reported in rodents and humans. For instance, the firing of hippocampal place cells is sequentially organized along the theta cycle during spatial navigation in rats (18). While such phase precession reflects physical proximity, our data show that theta phase-locked activity can also represent more abstract semantic information in humans. This is consistent with recent studies revealing task-dependent phase coding of varied neural representations in the hippocampus, including sequence learning of letters in working memory (20) and images in an episodic memory paradigm (21). A recent study demonstrated that representations of similar goal locations are locked to more distant hippocampal theta phases during virtual navigation (30), consistent with our finding of phase-based segregation of semantically similar items. This multitude of representational contents across experimental paradigms suggests a generic phase coding mechanism relying on mixed selectivity of hippocampal neurons (43, 44) that can be flexibly mapped onto different variables depending on task demands. Critically, our findings reveal the coexistence of two complementary systems for the representation of item-specific and semantic information during episodic memory retrieval: While distributed oscillatory patterns support the representation of individual items, the temporal structure of these signals is defined by a hippocampal theta phase code that preserves their semantic relations. The simultaneous expression of semantic and episodic memory codes might benefit memory by facilitating the accessibility of information according to task demands and enabling the integration of novel information into hierarchically organized mental schemas (45).

Beyond structuring stimulus-specific ERS dynamics, our data suggest that theta oscillations comprise two separate time windows for encoding and retrieval, in line with theoretical predictions (38) and recent experimental data in rodents (37) and humans (31). While our data seem consistent with these observations—ERS reductions at encoding occurred 160° away from those observed at retrieval—we note that the reductions at encoding did not reach statistical significance after stringent correction for multiple comparisons. Critically, our results revealed a difference in the angular means of active and passive conditions at retrieval, suggesting that volition induced the use of different theta slots for processing information under these two learning modes in addition to the overall encoding retrieval modulation.

Our results demonstrate simultaneous phase coding and phase clustering of ERS signals, i.e., segregation of mnemonic representations according to both their semantic content and their information processing mode (encoding or retrieval). We note that these phenomena have been reported at different temporal resolutions (i.e., with theta phase "slots" of varying length). In phase precession, for instance, the timing of unit firing is seen as a continuous variable that occurs across the entire theta cycle (18), while the standard view of phase coding during working memory assumes a maximal number of nested gamma cycles within a theta cycle reflecting memory capacity (46). Other studies have shown a distinction between early and late theta phases for representing current and alternative scenarios, respectively (19). The theory of an "optimal" oscillatory phase for encoding and retrieval, on the other hand, suggests a rather binary allocation of theta phase windows for these two information processing modes (38). Consistently, we observed a relatively large phase window of 126° reflecting the rising phase of the oscillation that was critically important for memory reactivations during retrieval. While phase clustering might reflect a general information processing mode requiring more extended theta slots for encoding and retrieval, phase coding might need a higher temporal resolution to structure high-level conceptual information. The cooccurrence of these mechanisms nevertheless suggests a multilayered system for efficient mnemonic processing supported by hippocampal theta oscillations, in which neural representations can be temporally assigned to distinct oscillatory phases of varying length according to their content, memory function (encoding vs. retrieval), and degree of volitional control (active or passive).

Our findings suggest that hippocampal signals do not play a key role in the representation of specific content, but rather coordinate item-specific representational patterns. Indeed, when ERS was calculated after removing hippocampal channels, no significant reductions in item-specific activity were observed (*SI Appendix*, Fig. S7). However, hippocampal theta oscillations facilitated the retrieval of item-specific information by providing a temporal scaffold for their representation, as our phase clustering (Fig. 5) and phase coding (Fig. 6) results demonstrated. Together, our data support a view of hippocampal theta as an evolutionary old navigational signal that evolved to support "navigation" in abstract and cognitive spaces (47, 48). We note though that the frequency range of human hippocampal theta (3–8 Hz) differs from the band typically reported in rodents (4–12 Hz), and appears to coordinate a semantic space following a more complex metric than space alone (11, 12).

We further investigated whether oscillatory power at individual electrodes reflected the relevance of these electrodes to item-specific representations. During encoding, electrodes with higher theta power contributed more to global representational patterns, even though these patterns did not rely on the amount of theta power in these electrodes (Fig. 4). During retrieval, electrodes with low beta and high gamma power were most relevant for item-specific reinstatement. These findings add to studies that recently tracked the frequency profile of reinstatement in the human brain, reporting beta and gamma power decreases (34, 35), together with increased high gamma (36) and "ripple" activity (33), as markers of the fidelity of stimulus-specific memory representations.

We note that the concept of "active learning" involves a multitude of interrelated cognitive functions including (but not limited to) decision making, active sampling, and exploration. In our operationalization of active learning, we chose a rather broad and naturalistic approach that aimed to optimize ecological validity at the expense of reduced control over individual cognitive variables. Possibly, such broad and flexible deployment of several intertwined cognitive processes is critical to engage the fine-grained mechanisms of phase coding and item-specific reinstatement that we found for actively learned items. Future studies will need to disentangle the contributions of these individual components of active learning. At the same time, further investigations using ecologically valid methods such as portable iEEG/MEG, eye tracking, or immersive virtual reality will be required to bridge the gap between an understanding of active

learning at the level of neurocognitive mechanisms and its practical application, e.g., in the context of education.

Single-unit studies revealed the importance of the time of firing with respect to hippocampal theta phase for memory processes (49) and their tuning to abstract representations irrespective of perceptual modalities (i.e., so-called "concept cells") (50). To our knowledge, no previous study has linked these two seemingly unrelated processes. We here provide evidence for a temporal organization of electrophysiological patterns that represent specific stimuli according to their semantic content. Our results describe a multiscale mnemonic phase code across the hippocampus and neocortex that links volition, item-specific and semantic representations, and the process of episodic memory.

Materials and Methods

Participants. Thirteen epilepsy patients (7 males, age = 33.5 ± 9.32) implanted with depth electrodes as part of their diagnostic assessment for medically refractory epilepsy participated in our experiment. Patients' demographic and clinical data are presented in *SI Appendix*, Table S1. The same paradigm was also conducted with a group of $n = 23$ healthy controls (17 males, age = 26.66 ± 9.62), who were students from the Universitat Pompeu Fabra (Barcelona, Spain). The study was approved by the local ethics committee, "Clinical Research Ethical Committee (CEIC) Parc de Salut Mar." Participants provided written informed consent to participate in the experiment.

Task Description. Subjects navigated a squared virtual environment in which images (see ref. 51) were presented at specific vertices of a 5 × 5 grid formed by red boxes located on the ground (Fig. 1 *A* and *B*). An item was presented at each box during navigation through a small inset on the top-right corner of the screen (Fig. 1*B*). The item remained visible until participants moved to another box. Participants were instructed to visit all boxes and remember all items for a subsequent recognition memory test.

Subjects explored the environment under two conditions, one with self-initiated, active control of movement (active) and the other via passive exposure and no control over navigation (passive). The navigation sequence in passive blocks—including trajectory information and items explored—was taken from the active mode of a matched pair from either our group of patients or from the healthy subjects control group, following a "yoked" design (Fig. 1 *C* and *D*).

Each subject performed three active and three passive navigation blocks. The order of the blocks was predefined, starting either with active or passive and then alternating. The starting block was counterbalanced across subjects: In total, eight patients started with the active block (A-P-A-P-A-P) and five with the passive block (P-A-P-A-P-A). The first subject in our study performed a shorter version of the task, with two active and two passive blocks instead of three.

Navigation blocks lasted for 3 min, with a 20-s pause after each block (Fig. 1*C*). The positions at the start of each active block were randomly selected from four possible predefined starting points covering four equally sized quadrants in the environment.

After the navigation period, subjects were tested for their memory using a recognition test (Fig. 1*E*). An image was displayed on the screen and subjects were asked to indicate whether they had seen it before using a confidence scale from 1 (sure new) to 6 (sure old, Fig. 1*E*). The confidence question (and the image) remained visible until participants gave a response, followed by an intertrial interval of 3 s.

Patients performed the experiment while sitting in their hospital beds using a 17-inch portable computer placed on a mobile tabletop. In the active condition, they controlled navigation with a joystick. The VR application was created with the Unity3D Game Engine.

Electrophysiological Recordings. Recordings were performed using a standard clinical EEG system (XLTEK, subsidiary of Natus Medical) with 500-Hz sampling rate. Dixi Médical electrodes (diameter: 0.8 mm; 5–15 contacts, 2 mm long, 1.5 mm apart) were stereotactically implanted using robotic guidance (ROSA, Medtech Surgical Inc.).

Electrode Selection. The presence of electrodes within the anterior hippocampus was confirmed via careful examination of the magnetic resonance imaging (MRI) and computed tomography (CT) scans with the help of our clinical team at the Hospital del Mar (Barcelona, Spain). Eleven out of 13 participants had at least one anterior hippocampal contact (range, 1–3 contacts). However, 2 of these 11 participants had to be excluded from the hippocampal analyses because the seizure onset zone was found in the anterior hippocampus. We selected the most distal anterior hippocampal contact when more than one was available in each subject.

Electrode locations in native space were determined using FreeSurfer (52) and converted to Montreal Neurological Institute (MNI) coordinates using the pipeline described in ref. 53. Only electrodes located in gray matter were included in the multielectrode (global) ERS analyses (see below). A full list of electrodes used and their MNI coordinates is provided in Dataset S1.

Artifact Rejection and Data Preprocessing. Before performing the artifact rejection, we removed all channels which were identified as the epileptogenic seizure onset zone (SOZ) by our clinical team, leaving 392 contacts that could be used for analyses (per patient ranging from 16 to 62 contacts). Artifact rejection on the remaining channels was then performed in two steps. We first applied an automatic procedure in which we automatically removed values beyond 5 SDs from the channel-specific mean (data from the full experiment) in both amplitude and gradient. We then epoched the data from −500 ms to 1.5 s after stimulus onset (mean exposure time to stimulus during encoding across all subjects = 1.44 s, SD = 0.35) and plotted event-related spectral perturbations (ERSPs) from all trials to evaluate the possible presence of noise in the time-frequency domain. Noisy trials were excluded by visual artifact rejection. This was done blindly with respect to the conditions of the experiment. In addition, all trials with an exposure time at encoding or a response time at retrieval of less than 200 ms or above 5 SD of the subject-specific mean were excluded. Data from rejected epochs was not only removed from the trial-based analysis but also from the analysis involving navigation blocks.

In total, this resulted in the following total number of trials in each condition: Item-specific analysis: 125.6 ± 47.7, volitional condition: 65.1 ± 30.7, passive condition: 60.4 ± 22.3, high confidence remembered condition: 82.76 ± 49.2, forgotten condition: 24.3 ± 13.6. The total number of trials in the item-specific ERS analysis after averaging revisits was 59.3 ± 12.9. For the phase coding analysis, an average of 2.55 ± 1.55 items of the labels provided in our stimulus set were not available in the word2vec embeddings (see below). Those were excluded from this specific analysis.

After artifact rejection, we band-pass filtered the signal at the selected electrodes from 1 to 200 Hz using a Hamming-windowed sinc finite impulse response filter (eegfiltnew.m from the EEGLAB toolbox) (54), and rereferenced the data to bipolar references before performing subsequent analyses. Bipolar referencing was done by subtracting the activity of one channel with that from the nearest channel of the same electrode, leading to a total of N-1 virtual contacts for an electrode with N contact points.

Hippocampal Power Analysis. We quantified hippocampal low-frequency power during the encoding phase of our experiment in the active and the passive navigation condition. Using the FieldTrip toolbox (55), we decomposed the signal during the whole experiment via complex Morlet wavelets with a variable number of cycles, linearly increasing between 3 cycles (at 1 Hz) to 6 cycles (at 29 Hz) in 29 steps for the low-frequency range, and from 6 cycles (at 30 Hz) to 12 cycles (at 150 Hz) in 25 steps for the high-frequency range. The resulting time series were Z-scored by taking the mean and SD of each frequency independently during all navigation blocks combined (three active and three passive).

We also analyzed differences in hippocampal theta power during retrieval of items that were encoded either actively or passively. We used the same parameters for time-frequency decomposition as in the encoding analysis, but retrieval trials were Z-scored to the concatenated activity of all periods of item-specific ERS (one per trial) combined.

We corrected all results on hippocampal theta oscillations presented in Fig. 2 for multiple comparisons using the Bonferroni method. Given that we tested six different frequency bands, we only considered P values significant that were below an alpha of 0.05/6.

Multielectrode (Global) ERS Analysis. We quantified the similarity of neural representations during encoding and retrieval by comparing epochs of brain activity across all available electrodes of each subject (56). We first calculated oscillatory power between 1 and 150 Hz for each trial using the same parameters as in the hippocampal power analysis (Morlet wavelets, 1-Hz steps from 1 to 29 Hz, 5-Hz steps from 30 to 150 Hz). We Z-scored the power time series in each trial by taking as a reference the activity of a period of −2 s before stimulus onset until 2 s after stimulus onset. Subsequently we extracted power values at 10 time points in windows of 500 ms (50-ms steps), starting at −500 ms and until 1.5 s after cue presentation. Consecutive windows incremented in steps of 50 ms. Similar to previous studies (32, 36), we calculated Spearman's correlations of broadband (1–150 Hz) oscillatory

patterns of activity across time, frequencies, and electrodes, resulting in a global measure of ranked similarity between encoding and retrieval (ERS). A representational feature vector therefore consisted of concatenated power values of 54 (frequencies) × 10 (time points) × n (subject-specific number of electrodes). Control analyses confirmed that similar results were obtained when feature vectors contained only information across frequencies and electrodes (i.e., not across time courses; see *SI Appendix*, Fig. S8).

We compared these feature vectors during all encoding and retrieval time windows using Spearman's rho (29, 34). Rho values at each time step were Fisher z-transformed for statistical comparisons. This resulted in an encoding × retrieval reinstatement map for each trial and subject, including both nonlagged (on-diagonal) and lagged (off-diagonal) correlations (Fig. 3*B*). These maps were subsequently contrasted via paired t tests across experimental conditions (Fig. 3*C*).

To assess a possible role of theta oscillations (3–8 Hz) as features in ERS, we performed the same multielectrode ERS analysis either with all frequencies except the theta band (Fig. 4 *A*, *Top*) or by excluding all frequencies except theta (Fig. 4 *A*, *Bottom*).

ERS Contrast Analyses. To identify stimulus-specific reinstatement, we compared encoding retrieval similarity of each item with the similarity between encoding of one item and retrieval of different items. Given that our experiment allowed participants to freely explore the items (in the active condition), some images were visited repeatedly. In these cases, each instance was considered separately, i.e., we correlated encoding activity of each visit of an item with the activity during retrieval of that item and counted them as "same item" correlations. Similar results were obtained when we averaged encoding activity across revisits before performing the ERS analysis (*SI Appendix*, Fig. S9). We randomly selected 1,000 instances of correlations between encoding of one item and retrieval of a different item in each subject. Alternatively, we matched the number of trials in the "different item" condition to that of the same item condition for each subject independently by randomly sampling from all possible combinations of items and averaging the results 100 times. This control rendered equivalent results. We calculated ERS for all selected pairs of same and different items across all time points and trials for each subject before performing statistical analyses at the group level.

To assess the behavioral relevance of stimulus-specific reactivations, we compared ERS values of high-confidence remembered vs. forgotten trials in a tROI defined by the results of the item-specific contrast (Fig. 3*C*; results in this tROI were first averaged in each participant). We also explored ERS differences between active and passive conditions using this approach (Fig. 3*D*).

Electrode-Wise ERS Contribution/Power Correlation Analysis. We quantified the relative contribution of each electrode to item reinstatement through a jackknife procedure. Mean ERS was calculated across trials in the same vs. different item cluster after excluding each electrode one by one (36). The contribution of electrode j to the overall ERS was defined as: $p_j = \frac{ERS_{all} - ERS_{all-j}}{ERS_{all}}$, where ERS_{all-j} is the averaged similarity value over trials after leaving electrode j out and ERS_{all} is the average ERS value over trials with all electrodes included. These values were normalized for each subject independently by subtracting from the contribution of each electrode the value of the least contributing electrode and dividing the result by the value of the most contributing electrode minus the value of the least contributing electrode, as in: $p_{norm} = \frac{P - P_{min}}{P_{max} - P_{min}}$. This normalization results in values between 0 and 1, where 0 corresponds to the least contributing electrode and 1 to the most contributing electrode of each subject.

In addition, we identified electrodes that were activated by the task at encoding using a previously described procedure (57). Power values at each frequency and electrode were Z-scored relative to a bootstrapped baseline period (−500 ms until item onset). The baseline was created by randomly sampling one power estimate per trial from the prestimulus baseline period and averaging the results. This was repeated 1,000 times, resulting in a surrogate distribution of baseline power values. Poststimulus power values (one value for every 50 ms) in each trial were Z-scored by taking as a reference the mean and SD of this bootstrapped distribution.

The mean Z-scored power values of each frequency during the first 500 ms after cue onset at encoding and retrieval were correlated with the contribution of each electrode to ERS (Fig. 4*C*). This correlation yielded one rho value per subject reflecting the relationship between the activity of each electrode and its contribution to the global ERS. These values were then compared against chance (i.e., zero) at the group level to assess statistical significance and corrected for multiple comparisons using cluster-based permutation statistics (see below).

Phase Clustering Analysis. To study whether specific phases of the hippocampal theta oscillation are particularly relevant for memory reactivations, we compared ERS with and without the values from individual phase bins across different conditions (Fig. 5*A*). We extracted power values at each electrode at an increased temporal resolution with respect to the main analysis (i.e., 10 ms) and built representational feature vectors by averaging frequency- and electrode-specific power values across consecutive time windows of 500 ms (overlapping by 450 ms), after excluding phase information of each specific bin of 18° (a total number of 20 bins) covering the full cycle. We used a relatively large number of phase bins given the requirements of cluster-based permutation statistics (see below). We did not include time in the feature vectors because the time periods that corresponded to the individual hippocampal theta phase bins were discontinuous, and therefore a continuously evolving reinstatement of neural activity time courses was not expected a priori. For each of these 500-ms time windows, we thus obtained a two-dimensional representational pattern composed of electrode x frequency values. We confirmed that we could again find significant item-specific ERS as in the main time-resolved analysis within this new tROI (*SI Appendix*, Fig. S8).

The contrast of same-item ERS vs. different-item ERS was then calculated, including ERS values across the full theta cycle, from which we subtracted ERS values from a single phase bin. This resulted in one averaged value of ERS reduction for each participant and phase bin, reflecting the contribution of that phase bin to the overall ERS effect. Statistical significance was assessed with paired t tests against zero applied to each phase bin (one-tailed tests were used given the hypothesis of increased ERS reduction after the removal of information in specific phase bins). We corrected for multiple comparisons using cluster-based permutation statistics (see below).

This analysis was first conducted separately for encoding and retrieval, and then further split up into the active and the passive condition. For all the encoding analyses, the encoding feature vector was modified according to the values of the hippocampal theta phase at encoding while the retrieval feature vector was left intact. The reverse was done in the retrieval analyses, leaving the encoding vector unmodified. To evaluate differences in the angular means of ERS reductions between encoding and retrieval, we applied Hotelling tests (58).

Phase Coding Analyses. We investigated whether the semantic content of a stimulus is encoded in the temporal relationship between the item-specific reinstatement (i.e., ERS) of this stimulus and hippocampal theta phases. We calculated a measure of representational similarity based on the semantic labels provided in our line drawings dataset (51). These labels were compared between all pairs of items using Google's word2vec (40), a method for generating vector representations of words which provides a pretrained set of 300-dimensional embeddings based on a large Google News text corpus. A semantic similarity measure was extracted for each pair of images by correlating word2vec vector representations using Spearman's rho. The resulting confusion matrix was then correlated with neural similarity matrices of phase-dependent reinstatement of stimulus-specific information (Fig. 6*B*). To produce these neural similarity matrices, we first generated representational feature vectors at increased temporal resolution as in the phase clustering analysis (i.e., 10 ms) and band-pass filtered the hippocampal activity between 3 and 8 Hz to extract a time series of instantaneous phases using the Hilbert transform. The phase time series were then downsampled to 100 Hz to match the temporal resolution of the ERS data (Fig. 6*A*). We verified that we could still capture item-specific representations at this temporal resolution (*SI Appendix*, Fig. S11), and then split the hippocampal theta phase time series of each trial during the period of item reinstatement (cluster defined in the main analysis, Fig. 3*C*) into 10 equally sized phase bins of 36° each (31). Average ERS values from 1,000 draws in the different item condition were subtracted from the same item condition at each trial, to avoid any bias related to unspecific (i.e., not stimulus-specific) ERS. We then calculated the mean ERS in each phase bin, resulting in one distribution of item-specific ERS values across hippocampal theta phases for each trial. ERS phase distributions were compared between all pairs of trials using the circular correlation from the CircStats toolbox (59). This was done separately during encoding and retrieval, resulting in two neural similarity matrices in each patient. We removed values on the diagonal of both matrices, to avoid inflating results due to correlation values of 1 on the diagonal of the word2vec matrix. We also excluded values at one side of the diagonal in both matrices given their symmetry. Note that in the examples presented in Fig. 6*B* circular correlation values were sign changed for visualization.

We correlated the semantic similarity matrix with the participant-wise neural similarity matrix using Spearman's rho. At the group level, the resulting individual rho values were compared against chance, i.e., zero

using a one-sample t test. Note that in the results presented in Fig. 6*C*, resulting rho values were sign changed for visualization. Statistical significance was assessed by randomly shuffling the labels of the neural and the word2vec similarity matrices 1,000 times before correlating them and performing the second-level statistics, resulting in a distribution of t values under the null hypothesis of no phase-ERS relationship. We considered significant an observed t value falling above the 95th percentile of this shuffled distribution.

Several control analyses were performed to corroborate the results of the phase coding analysis (*SI Appendix, Supplementary Methods*).

Multiple Comparisons Correction. We performed cluster-based permutation statistics to correct for multiple comparisons in the main ERS analysis (Fig. 3), in the electrode-wise ERS contribution/power correlation analysis (Fig. 4), and in the phase clustering analysis (Fig. 5).

In the ERS analysis, we created a null distribution of ERS values by permuting the labels of the trials for each subject independently 1,000 times. Paired t tests were then applied in sliding 500-ms windows with incremental steps of 50 ms on the surrogate data (as for the empirical data). We identified clusters of contiguous significant time windows (corresponding to P values <0.05) and selected the maximum cluster size of summed t values for every permutation. This resulted in a distribution of surrogate t values for every encoding time × retrieval time point under the assumption of the null hypothesis. We only considered significant those contiguous encoding retrieval time pairs in the nonshuffled data whose summed t values exceeded the summed t value of 95% of the distribution of surrogate clusters (corresponding to a corrected $P < 0.05$) (60).

In the analysis comparing the electrode-wise ERS contributions to electrode-wise power, we used cluster statistics to correct for multiple comparisons across frequencies (Fig. 4). We shuffled the assignment of electrode identity for power and for electrode contribution to ERS 1,000 times. We identified in each permutation the largest cluster of contiguous frequencies that were significant ($P < 0.05$) in the comparison of correlation (rho) values against zero at the group level. This yielded a distribution of correlation clusters (across frequencies) that could be expected by chance. We tested whether the observed correlation cluster exceeded the 95th percentile of this distribution.

In the phase clustering analysis, we generated a chance distribution of ERS reductions by randomly shuffling the trial ID of hippocampal phase and ERS signals 1,000 times. At each permutation, we recalculated ERS reductions after the removal of ERS at specific phases and looked for the biggest cluster of contiguous significant phase bins. Phase bins at the extremes of the cycle were grouped into clusters when necessary, given the circular nature of the data. Statistical significance was calculated by comparing the observed t value with respect to this surrogate distribution.

Data Availability. Anonymized intracranial EEG data and custom-written Matlab code supporting the findings of this study are available in Open Science Framework at https://osf.io/j582a/.

ACKNOWLEDGMENTS. We thank Nora Herweg for providing feedback on an earlier version of the manuscript, Sytse Wierenga for his help with the production of figures, and Martí Sánchez Fibla and Bryan Strange for discussions related to the manuscript. This work has received funding from the Horizon2020-EU program under grant agreement of the project ReHyb, ID: 871767, and from the Virtual Brain Cloud project under the program H2020-EU, ID: 826421. N.A. received funding from Deutsche Forschungsgemeinschaft (German Research Foundation) Projektnummer 316803389–SFB 1280, as well as via Projektnummer 122679504–SFB 874.

1. I. Fried, P. Haggard, B. J. He, A. Schurger, Volition and action in the human brain: Processes, pathologies, and reasons. *J. Neurosci.* **37**, 10842–10847 (2017).
2. T. M. Gureckis, D. B. Markant, Self-directed learning: A cognitive and computational perspective. *Perspect. Psychol. Sci.* **7**, 464–481 (2012).
3. D. B. Markant, A. Ruggeri, T. M. Gureckis, F. Xu, Enhanced memory as a common effect of active learning. *Mind Brain Educ.* **10**, 142–152 (2016).
4. N. Rotem-Turchinski, A. Ramaty, A. Mendelsohn, The opportunity to choose enhances long-term episodic memory. *Memory* **27**, 431–440 (2019).
5. V. P. Murty, S. DuBrow, L. Davachi, The simple act of choosing influences declarative memory. *J. Neurosci.* **35**, 6255–6264 (2015).
6. P. F. M. J. Verschure, T. Voegtlin, R. J. Douglas, Environmentally mediated synergy between perception and behaviour in mobile robots. *Nature* **425**, 620–624 (2003).
7. P. Haggard, The neurocognitive bases of human volition. *Annu. Rev. Psychol.* **70**, 9–28 (2019).
8. J. L. Voss, B. D. Gonsalves, K. D. Federmeier, D. Tranel, N. J. Cohen, Hippocampal brain-network coordination during volitional exploratory behavior enhances learning. *Nat. Neurosci.* **14**, 115–120 (2011).
9. H. T. Ito, S.-J. Zhang, M. P. Witter, E. I. Moser, M.-B. Moser, A prefrontal-thalamo-hippocampal circuit for goal-directed spatial navigation. *Nature* **522**, 50–55 (2015).
10. H. Eichenbaum, Prefrontal-hippocampal interactions in episodic memory. *Nat. Rev. Neurosci.* **18**, 547–558 (2017).
11. C. H. Vanderwolf, Hippocampal electrical activity and voluntary movement in the rat. *Electroencephalogr. Clin. Neurophysiol.* **26**, 407–418 (1969).
12. L. L. Colgin, Rhythms of the hippocampal network. *Nat. Rev. Neurosci.* **17**, 239–249 (2016).
13. R. Kaplan *et al.*, Movement-related theta rhythm in humans: Coordinating self-directed hippocampal learning. *PLoS Biol.* **10**, e1001267 (2012).
14. A. Goyal *et al.*, Functionally distinct high and low theta oscillations in the human hippocampus. *Nat. Commun.* **11**, 2469 (2020).
15. Z. M Aghajan *et al.*, Theta oscillations in the human medial temporal lobe during real-world ambulatory movement. *Curr. Biol.* **27**, 3743–3751.e3 (2017).
16. V. D. Bohbot, M. S. Copara, J. Gotman, A. D. Ekstrom, Low-frequency theta oscillations in the human hippocampus during real-world and virtual navigation. *Nat. Commun.* **8**, 14415 (2017).
17. J. E. Lisman, O. Jensen, The θ-γ neural code. *Neuron* **77**, 1002–1016 (2013).
18. W. E. Skaggs, B. L. McNaughton, M. A. Wilson, C. A. Barnes, Theta phase precession in hippocampal neuronal populations and the compression of temporal sequences. *Hippocampus* **6**, 149–172 (1996).
19. K. Kay *et al.*, Constant sub-second cycling between representations of possible futures in the hippocampus. *Cell* **180**, 552–567.e25 (2020).
20. A. Bahramisharif, O. Jensen, J. Jacobs, J. Lisman, Serial representation of items during working memory maintenance at letter-selective cortical sites. *PLoS Biol.* **16**, e2003805 (2018).
21. A. C. Heusser, D. Poeppel, Y. Ezzyat, L. Davachi, Episodic sequence memory is supported by a theta-gamma phase code. *Nat. Neurosci.* **19**, 1374–1380 (2016).
22. T. Staudigl, S. Hanslmayr, Theta oscillations at encoding mediate the context-dependent nature of human episodic memory. *Curr. Biol.* **23**, 1101–1106 (2013).
23. H. Sanders, C. Rennó-Costa, M. Idiart, J. Lisman, Grid cells and place cells: An integrated view of their navigational and memory function. *Trends Neurosci.* **38**, 763–775 (2015).
24. M. Leszczyński, J. Fell, N. Axmacher, Rhythmic working memory activation in the human hippocampus. *Cell Rep.* **13**, 1272–1282 (2015).
25. N. Axmacher *et al.*, Cross-frequency coupling supports multi-item working memory in the human hippocampus. *Proc. Natl. Acad. Sci. U.S.A.* **107**, 3228–3233 (2010).
26. R. T. Canolty *et al.*, High gamma power is phase-locked to theta oscillations in human neocortex. *Science* **313**, 1626–1628 (2006).
27. T. Schreiner, T. Staudigl, Electrophysiological signatures of memory reactivation in humans. *Philos. Trans. R. Soc. Lond. B Biol. Sci.* **375**, 20190293 (2020).
28. B. P. Staresina, M. Wimber, A neural chronometry of memory recall. *Trends Cogn. Sci.* **23**, 1071–1085 (2019).
29. D. Pacheco Estefan *et al.*, Coordinated representational reinstatement in the human hippocampus and lateral temporal cortex during episodic memory retrieval. *Nat. Commun.* **10**, 2255 (2019).
30. L. Kunz *et al.*, Hippocampal theta phases organize the reactivation of large-scale electrophysiological representations during goal-directed navigation. *Sci. Adv.* **5**, eaav8192 (2019).
31. C. Kerrén, J. Linde-Domingo, S. Hanslmayr, M. Wimber, An optimal oscillatory phase for pattern reactivation during memory retrieval. *Curr. Biol.* **28**, 3383–3392.e6 (2018).
32. R. B. Yaffe *et al.*, Reinstatement of distributed cortical oscillations occurs with precise spatiotemporal dynamics during successful memory retrieval. *Proc. Natl. Acad. Sci. U.S.A.* **111**, 18727–18732 (2014).
33. H. Zhang, J. Fell, N. Axmacher, Electrophysiological mechanisms of human memory consolidation. *Nat. Commun.* **9**, 4103 (2018).
34. B. P. Staresina *et al.*, Hippocampal pattern completion is linked to gamma power increases and alpha power decreases during recollection. *eLife* **5**, e17397 (2016).
35. B. J. Griffiths *et al.*, Alpha/beta power decreases track the fidelity of stimulus-specific information. *eLife* **8**, e49562 (2019).
36. H. Zhang *et al.*, Gamma power reductions accompany stimulus-specific representations of dynamic events. *Curr. Biol.* **25**, 635–640 (2015).
37. M. E. Hasselmo, C. E. Stern, Theta rhythm and the encoding and retrieval of space and time. *Neuroimage* **85**, 656–666 (2014).
38. M. E. Hasselmo, C. Bodelón, B. P. Wyble, A proposed function for hippocampal theta rhythm: Separate phases of encoding and retrieval enhance reversal of prior learning. *Neural Comput.* **14**, 793–817 (2002).
39. E. A. Solomon, B. C. Lega, M. R. Sperling, M. J. Kahana, Hippocampal theta codes for distances in semantic and temporal spaces. *Proc. Natl. Acad. Sci. U.S.A.* **116**, 24343–24352 (2019).
40. T. Mikolov, K. Chen, G. Corrado, J. Dean, Efficient estimation of word representations in vector space. arXiv:1301.3781 (2013).
41. E. Y. Song, Y. B. Kim, Y. H. Kim, M. W. Jung, Role of active movement in place-specific firing of hippocampal neurons. *Hippocampus* **15**, 8–17 (2005).
42. G. Buzsáki, Theta rhythm of navigation: Link between path integration and landmark navigation, episodic and semantic memory. *Hippocampus* **15**, 827–840 (2005).
43. S. McKenzie *et al.*, Representation of memories in the cortical-hippocampal system: Results from the application of population similarity analyses. *Neurobiol. Learn. Mem.* **134**, 178–191 (2016).

44. N. A. Cruzado, Z. Tiganj, S. L. Brincat, E. K. Miller, M. W. Howard, Conjunctive representation of what and when in monkey hippocampus and lateral prefrontal cortex during an associative memory task. *Biorxiv* 709659 (2019).
45. D. Tse *et al*., Schemas and memory consolidation. *Science* **316**, 76–82 (2007).
46. J. E. Lisman, M. A. Idiart, Storage of 7 +/- 2 short-term memories in oscillatory subcycles. *Science* **267**, 1512–1515 (1995).
47. J. L. S. Bellmund, P. Gärdenfors, E. I. Moser, C. F. Doeller, Navigating cognition: Spatial codes for human thinking. *Science* **362**, eaat6766 (2018).
48. G. Buzsáki, E. I. Moser, Memory, navigation and theta rhythm in the hippocampal-entorhinal system. *Nat. Neurosci.* **16**, 130–138 (2013).
49. U. Rutishauser, I. B. Ross, A. N. Mamelak, E. M. Schuman, Human memory strength is predicted by theta-frequency phase-locking of single neurons. *Nature* **464**, 903–907 (2010).
50. R. Q. Quiroga, Concept cells: the building blocks of declarative memory functions. *Nat. Rev. Neurosci.* **13**, 587–597 (2012).
51. B. Rossion, G. Pourtois, Revisiting snodgrass and vanderwart's object pictorial set: The role of surface detail in basic-level object recognition. *Perception* **33**, 217–236 (2004).
52. B. Fischl, FreeSurfer. *Neuroimage* **62**, 774–781 (2012).
53. A. Stolk *et al*., Integrated analysis of anatomical and electrophysiological human intracranial data. *Nat. Protoc.* **13**, 1699–1723 (2018).
54. A. Delorme, S. Makeig, EEGLAB: An open source toolbox for analysis of single-trial EEG dynamics including independent component analysis. *J. Neurosci. Methods* **134**, 9–21 (2004).
55. R. Oostenveld, P. Fries, E. Maris, J.-M. Schoffelen, FieldTrip: Open source software for advanced analysis of MEG, EEG, and invasive electrophysiological data. *Comput. Intell. Neurosci.* **2011**, 156869 (2011).
56. N. Kriegeskorte, M. Mur, P. Bandettini, Representational similarity analysis - connecting the branches of systems neuroscience. *Front. Syst. Neurosci.* **2**, 4 (2008).
57. S. M. Szczepanski *et al*., Dynamic changes in phase-amplitude coupling facilitate spatial attention control in fronto-parietal cortex. *PLoS Biol.* **12**, e1001936 (2014).
58. J. H. Zar, *Biostatistical Analysis* (Pearson Education India, 1999).
59. P. Berens, CircStat: A MATLAB toolbox for circular statistics. *J. Stat. Softw.* **31**, 1–21 (2009).
60. E. Maris, R. Oostenveld, Nonparametric statistical testing of EEG- and MEG-data. *J. Neurosci. Methods* **164**, 177–190 (2007).